Crystal Structure of a Ternary Complex of the Alcohol Dehydrogenase from *Sulfolobus solfataricus*[†,‡]

Luciana Esposito,[§] Ilaria Bruno,[||] Filomena Sica,[§,⊥] Carlo Antonio Raia,[@] Antonietta Giordano,[@] Mosè Rossi,[||,@] Lelio Mazzarella,[§,⊥] and Adriana Zagari*[,§,||]

Istituto di Biostrutture e Bioimmagini, CNR, via Mezzocannone 6-8, I-80134 Napoli, Italy, Dipartimento di Chimica, Università degli Studi di Napoli "Federico II", via Cinthia, I-80126 Napoli, Italy, Istituto di Biochimica delle Proteine, CNR, via Marconi 10, I-80125 Napoli, Italy, and Dipartimento di Chimica Biologica, Università degli Studi di Napoli "Federico II", via Mezzocannone 6, I-80134 Napoli, Italy

Received July 18, 2003; Revised Manuscript Received October 2, 2003

ABSTRACT: The crystal structure of a ternary complex of the alcohol dehydrogenase from the archaeon *Sulfolobus solfataricus* (SsADH) has been determined at 2.3 Å. The asymmetric unit contains a dimer with a NADH and a 2-ethoxyethanol molecule bound to each subunit. The comparison with the apo structure of the enzyme reveals that this medium chain ADH undergoes a substantial conformational change in the apo−holo transition, accompanied by loop movements at the domain interface. The extent of domain closure is similar to that observed for the classical horse liver ADH, although some differences are found which can be related to the different oligomeric states of the enzymes. Compared to its apo form, the SsADH ternary complex shows a change in the ligation state of the active site zinc ion which is no longer bound to Glu69, providing additional evidence of the dynamic role played by the conserved glutamate residue in ADHs. In addition, the structure presented here allows the identification of the substrate site and hence of the residues that are important in the binding of both the substrate and the coenzyme.

Alcohol dehydrogenases (ADHs)[1] of the zinc-dependent medium chain dehydrogenase/reductase family are present in essentially all types of life forms, are involved in detoxification, and probably have more specific functions in higher eukaryotes (*1*). Dimeric ADHs usually occur in higher eukaryotes, whereas tetrameric ADHs are found in prokaryotes and lower eukaryotes. Since the early studies on horse liver alcohol dehydrogenase (HLADH) (*2*), the representative enzyme of this family, considerable knowledge of dimeric ADH three-dimensional (3D) structures has been gained (*3*−*5*). On the other hand, only a limited number of tetrameric ADH structures are available to date (*6*−*9*).

Each subunit in ADH structures comprises a catalytic domain and a coenzyme-binding domain which move relative to each other upon coenzyme binding. This domain movement, which results in a closure of the interdomain cleft, is a characteristic feature of dimeric ADHs. The different extent of conformational changes observed in several ADH structures determined so far gave further support to the early idea that there are intermediate conformational states between the fully "open" and the fully "closed" conformations of wild-type HLADH (*10*). These intermediate states could be trapped by the crystallization conditions being associated with different steps during the catalytic cycle, or else these conformations could be the functional ones for different members of the ADH family or for mutated ADH obtained by protein engineering. For instance, open conformations for holo-ADH forms have been suggested to be the active states in the case of an HLADH mutant (*11*), whereas partially closed conformations appear to be the case with the tetrameric bacterial TbADH. When the coenzyme binds, the latter enzyme did not exhibit conformational changes of the tertiary structure either in the X-ray structure of the binary complex with its cofactor (*6*) or in its ternary complex studied by spectroscopic techniques (*12*).

In addition to the domain orientation, other differences among the ADHs can be related to the coordination environment of the catalytic zinc ions. Indeed, in few recently determined structures, the tetrahedral arrangement of ligands around the zinc shows a coordinated Glu residue, usually found in the second coordination sphere (*6*−*9*). Furthermore, recent studies have suggested the possibility of a change in the zinc coordination from tetra- to pentacoordination during turnover, although no general agreement about the nature of this pentacoordinated intermediate exists (*12, 13*).

In this scenario, puzzling questions remain about the role of the different domain movements, the distinct types of zinc coordinations and their correlation to coenzyme binding and catalytic mechanisms, and the structural differences in oligomerization and its functional significance.

[†] This work was supported by grants from ASI (Agenzia Spaziale Italiana).

[‡] Coordinates of the model have been deposited in the Protein Data Bank (entry 1R37).

[§] Istituto di Biostrutture e Bioimmagini, CNR.

[||] Dipartimento di Chimica Biologica, Università degli Studi di Napoli "Federico II".

[⊥] Dipartimento di Chimica, Università degli Studi di Napoli "Federico II".

[@] Istituto di Biochimica delle Proteine, CNR.

[1] Abbreviations: ADH, alcohol dehydrogenase; SsADH and HLADH, *S. solfataricus* and horse liver ADH, respectively; rmsd, root-mean-square deviation; wt, wild-type; K_M, Michaelis constant; K_d, dissociation constant; NAD^+ and NAD(H), oxidized and reduced forms of β-nicotinamide adenine dinucleotide, respectively; NCS, noncrystallographic symmetry.

10.1021/bi035271b CCC: $25.00
Published on Web 11/20/2003

Table 1: Data Collection and Refinement Statistics

data collection	
resolution (Å)	25.0−2.3 (2.38−2.3)
space group	*C*2
cell dimensions	131.1 Å, 83.0 Å, 68.7 Å, 90°, 96.5°, 90°
no. of measured reflections/ no. of unique reflections	70105/29287
completeness (%)	89.5 (60.8)
R_{merge} (%)	5.8 (7.1)
$\langle I \rangle / \langle \sigma(I) \rangle$	14 (8.8)
solvent content (%)	50.2
refinement	
no. of non-zero reflections used in R/R_{free}	27610/1521
R (%)/R_{free} (%)	19.3/22.5
rmsd for bonds (Å)	0.006
rmsd for angles (deg)	1.61

To provide new insight into these issues, we have determined the structure of a holo form of *Sulfolobus solfataricus* ADH (SsADH). The 2-ethoxyethanol−NAD(H)−SsADH structure is the first ADH ternary complex from Archaea to be described. Here, the structure is compared with that of its corresponding apo form (*7*) as well as with other ADH structures, in particular with the classical dimeric HLADH enzyme. Furthermore, this complex allows the identification of the substrate site and hence of the residues that are important in the binding of both the substrate and the coenzyme.

MATERIALS AND METHODS

Crystallization and Data Collection. The SsADH enzyme was expressed and purified from *Escherichia coli* following the procedure described previously (*14*). Crystals of the holoenzyme were grown by sitting-drop vapor diffusion at 23 °C. An 8 mg/mL SsADH solution containing 2 mM NAD^+ and 10 mM 2,2,2-trifluoroethanol was equilibrated with 100 mM Na/K phosphate buffer (pH 6.2), 200 mM NaCl, and 40% (v/v) 2-ethoxyethanol. The final precipitant solution was derived from an optimization of the crystallization conditions found using the Emerald Biostructure CryoI kit. Diffraction data were collected at 110 K on freshly prepared crystals after 4 days of growth, using beamline ID14-4 of the ESRF synchrotron in Grenoble, France.

SsADH complexed with its coenzyme usually forms nonmerohedrally twinned crystals (*15*). Two reciprocal lattices which do not superimpose exactly can be indeed recognized in the diffraction pattern. They are related by a 180° rotation about the *a* axis. The majority of the crystals examined by X-ray were highly twinned. After several trials, the least twinned crystal was selected for data collection. The much stronger contribution to the diffraction pattern from one of the lattices ("lattice 1") allowed the automatic indexing and reducing of spots by the DENZO program (*16*). Approximately 1.1% (2217 of 206 701) of the observations were discarded because of the presence of additional spots from the other lattice, but most of the reflections were integrated with minor errors. The R_{merge} value is 5.8% for data in the resolution range of 25−2.3 (7.1% in 2.38−2.3 Å shell). Data collection statistics obtained with the DENZO/SCALEPACK package (*16*) are given in Table 1.

It was also possible to process data from the second lattice ("lattice 2") by imposing the crystal orientation derived by the previously identified twin law, in the automated data reduction. Because of the very poor quality of the data statistics for the second lattice, this data set was not used further. However, a rough estimate of the twin fractions in the crystal was derived simply by a scaling of the two intensity data sets, once the 0*kl* reflections, common to both lattices, were put on the same scale. The twinned crystal is formed by lattice 1 for ∼70% and by lattice 2 for the remaining 30%.

Structure Solution and Refinement. The structure was determined by the molecular replacement method using AMoRe (*17*) and the previously reported apo structure as the search model (PDB entry 1JVB) (*7*). In the calculations, the catalytic domain (residues 1−153 and 295−346 and two zinc ions) and the coenzyme-binding domain (residues 157−292) were treated independently of each other. The initial search was performed by using the coenzyme-binding domains of the AB dimer from apo-SsADH. Once this partial model was positioned, the two catalytic domains were searched sequentially. The complete solution comprising a dimer showed a correlation coefficient and *R*-factor of 53.4 and 42.8%, respectively, using data within 10−3.5 Å. The homotetramer is generated from the dimer in the asymmetric unit (a.u.), by the 2-fold crystallographic axis.

The refinement was carried out using the program CNS (*18*) with 5.5% of the reflections omitted for the calculation of R_{free}. Throughout the refinement, noncrystallographic (NCS) restraints were used. In the last refinement stages, NCS symmetry restraints of 80 and 10 kcal/mol were applied to the main chain and to the side chain atoms in the dimer, respectively.

Visual inspection of the models and the electron density maps during refinement was accomplished using the program O (*19*). The omit difference maps gave a very clear density for the coenzyme molecule since the early stages of refinement. Moreover, an elongated density was visible very close to the catalytic zinc ion. The shape of this density could not be fitted by a bulky molecule, such as 2,2,2-trifluoroethanol, but was instead well fitted by a linear chain, such as that of the 2-ethoxyethanol precipitant. Therefore, the 2-ethoxyethanol competed with the binding of 2,2,2-trifluoroethanol. In the final stages of the refinement, the former molecule was added to the model, directly bound to the zinc in both subunits. The final model shows *R*-factor and R_{free} values of 19.5 and 22.5%, respectively, calculated by using data between 25.0 and 2.3 Å. The stereochemistry of the model was validated with the program PROCHECK (*20*). Refinement statistics are summarized in Table 1.

Fluorescence Studies and Kinetic Characterization. A fluorimetric assay was used to detect the poor SsADH activity at relatively low temperatures using a JASCO FP-777 spectrofluorometer equipped with an external thermocryostated water bath. The assay mixture reproduced the crystallization conditions diluted by a factor of 100, i.e., 0.002 mM SsADH, 4.1 mM 2-ethoxyethanol, 0.02 mM NAD^+, 0.1 mM 2,2,2-trifluoroethanol, 1 mM Na/K phosphate buffer (pH 6.2), and 2 mM NaCl. The change in NADH fluorescence was recorded as a function of time, with λ_{ex} and λ_{em} fixed at 340 and 463 nm, respectively. The concentrations of NADH and NAD^+ at equilibrium were found to be 4 and 16 μM, respectively, at a temperature of 25 °C. The spectrophotometric determination of the kinetic constants for 2-ethoxy-

Table 2: Kinetic Constants of SsADH[a]

substrate	k_{cat} (s^{-1})	K_m (mM)	k_{cat}/K_m (s^{-1} mM^{-1})
benzyl alcohol	3.3	0.16	20.5
ethanol	3.1	4.6	0.67
1-propanol	3.6	0.61	5.88
1-butanol	2.8	0.14	20.5
1-pentanol	1.9	0.06	32.2
2-ethoxyethanol	0.5	0.77	0.65

[a] Kinetic constants were determined at 50 °C in 100 mM Gly/NaOH (pH 10.5) and 3 mM NAD^+.

ethanol at 25 or 50 °C and pH 6.2 was not feasible since this alcohol is a very poor substrate under these conditions. However, the kinetic constants of 2-ethoxyethanol, linear aliphatic alcohols, and benzyl alcohol were measured at 50 °C and pH 10.5 as shown in Table 2.

Coenzyme binding studies by fluorescence quenching (λ_{ex} = 280 nm) were also carried out, as described previously (*33*), to evaluate the dissociation constant (K_d) for both NAD^+−SsADH and NADH−SsADH binary complexes under temperature, pH, and ionic strength conditions used for crystallization. The K_d values obtained were 68 and 0.66 μM for NAD^+ and NADH, respectively.

Given the equilibrium concentration of NAD^+ and NADH in the crystallization mixture and the higher affinity of the enzyme for NADH, it can be suggested that the crystal contains the abortive complex, enzyme−NADH−alcohol. However, the presence of a mixture of oxidized and reduced cofactor cannot be ruled out.

RESULTS

Overall Structure of the SsADH Ternary Complex. The structure of the SsADH−NADH−2-ethoxyethanol ternary complex was determined at 2.3 Å resolution by molecular replacement, using the previously reported apo form of SsADH as the search model (*7*). The asymmetric unit comprises two monomers which form the typical dimer by connecting the β-sheets of their Rossmann folds. The NAD(H) and the 2-ethoxyethanol molecules are present in both subunits. All 347 residues of each chain were fitted into the electron density, and the final model also contains 204 ordered water molecules. Compared to that of the apoenzyme structure, the electron density of the holo form was significantly better defined, because of the greater compactness of the molecule as well as the tighter crystal packing. The model is of good quality, with only one residue, on both subunits (Val296), in the generously allowed regions of the Ramachandran plot.

Since the noncrystallographic symmetry relating the two subunits in the a.u. is strictly conserved, we refer to subunit A in the following discussion, unless otherwise stated.

Orientation and Structure Differences of the Domains. SsADH adopts different conformations in the apo form and the ternary complex, due to a movement of the catalytic domain toward the coenzyme-binding domain. Residues 155−295 are considered to belong to the coenzyme-binding domain, whereas residues 1−154 and 296−347 belong to the catalytic domain. To determine the extent of domain closure, the coenzyme-binding domain was aligned with that of the apoenzyme. The "closure" can be then described by the rigid-body rotation required to superimpose the catalytic domains. The SsADH catalytic domain of the apoenzyme must be rotated ~11° toward the coenzyme-binding domain, to match the catalytic domain of the holoenzyme (Figure 1A). C^α atoms were used in the superposition. The two subunits in the asymmetric unit show the same degree of domain movement. The "closed" conformation in the SsADH ternary complex is similar to that typically observed in binary and ternary complexes of class I eukaryotic ADHs (*21*).

When the coenzyme-binding domains of the apo and holo forms are superimposed separately using C^α atoms, the overall rmsd is 0.65 Å (Table 3). The only remarkable differences are found at positions 271−274 where the displacement of C^α atoms is greater than 1.5 Å and up to 3.8 Å. After removal of the eight residues deviating by more than 1.0 Å from the superposition, the rmsd decreases to 0.42 Å. Larger deviations (rmsd of 1.13 Å) are observed when the catalytic domains are aligned. In this case, the regions with differences greater than 2.0 Å include residues 47−60, 315−319, 340, and 341. The rmsd decreases to 0.52 Å when the 37 residues deviating by more than 1.2 Å are omitted from the superposition.

A similar analysis carried out on the HLADH apo and holo forms (PDB entries 8ADH and 2OHX, respectively) reveals that the conformation of the structural elements forming the catalytic domain is more internally conserved than in SsADH. In fact, the rmsd on all C^α atoms of the catalytic domains (residues 1−174 and 319−374) is only 0.44 Å. The coenzyme-binding domains (residues 175−318), once aligned, display an rmsd of 0.78 Å. By using a similar selection for deviating residues in HLADH superpositions (rmsd of >1 Å and rmsd of >0.9 Å are the cutoffs for eliminating residues from alignment of the coenzyme-binding and catalytic domains, respectively), even lower rmsds were obtained, i.e., 0.33 Å from both alignments.

Quaternary Structure of SsADH Forms. The quaternary structure in SsADH apo and holo forms was first analyzed and then compared to that of HLADH. The SsADH tetramer is a dimer of dimers (AB and CD) where each dimer is very similar to the HLADH structure which is assembled by the pairing of the six-stranded β-sheets of the coenzyme-binding domains to form an extended 12-stranded β-sheet. Dimers AB and CD interact by their sides opposite from the interdomain cleft, i.e., the "backside" of each subunit. The central core of the tetramer mainly consists of the AD (BC) interface with interactions involving residues of the coenzyme-binding domains (170, 171, 193−196, and 160) as well as helix α4 and the loop that follows in the catalytic domain. Helix α4 lies parallel to the interdomain crevice length. Although subunits A and D have a limited area of intersubunit contact (*7*), the AD interface is the best conserved in the tetramer upon apo−holo transition. In fact, the other interface between the A and C subunits is mainly associated with contacts involving regions of the catalytic domain as well as the same α4 helix which is also on the AD interface. The conformational rearrangement in the apo−holo transition leaves the core of the tetramer essentially unchanged. If the coenzyme-binding β-sheets of the AB dimer in holo-SsADH and apo-SsADH are superimposed, the equivalent β-sheets of the CD dimer are aligned within 3°. Thus, the structural rearrangement mainly involves the catalytic domains at the ends of the tetramer core. The different role played by the AD and AC interfaces in the apo−holo transition can also

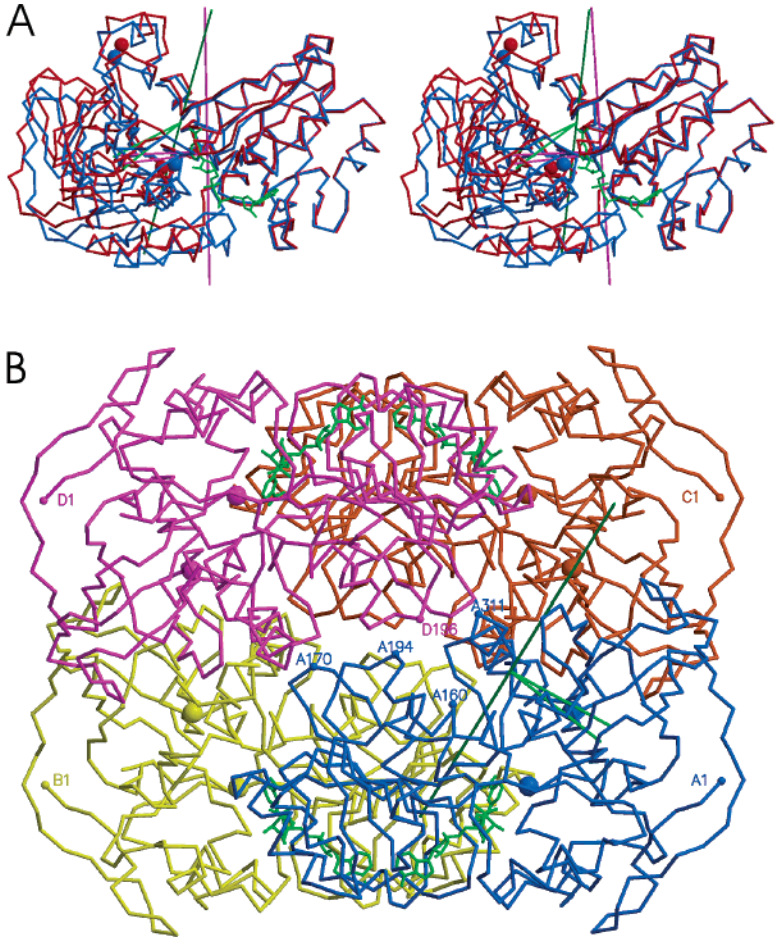

FIGURE 1: Structural changes in SsADH upon apo−holo transition. (A) Residues from the coenzyme-binding domain (A subunit) of the holo structure presented here were aligned with the corresponding residues in the apo structure (red). The rotation axis relative to the rigid-body movement of the catalytic domain toward the coenzyme-binding domain is in green. In addition, the position of the analogous rotation axis for the HLADH apo−holo transition is in magenta. The latter axis was obtained after having best aligned the HLADH holo structure (PDB entry 2OHX) with the SsADH holo structure by using C^{α} atoms of the structurally conserved residues belonging to both domains. (B) Tetramer structure of the holo form. A few residues at the core of the tetramer interface are highlighted. The rotation axis (green) is shown for only subunit A (blue). At the center of the molecule, the β-sheet of the coenzyme-binding domains also can be clearly identified by the NAD(H) molecules (green). This figure was generated by using MolScript (*44*) and Raster3D (*45*). The program FIT (L. Guoguang, unpublished) was used to visualize the rotation axes.

Table 3: Structural Comparisons by C^{α} Atom Alignments

	rmsd for C^{α} atoms (Å)	
superposition zone	apo-SsADH−holo-SSADH	apo-HLADH−holo-HLADH
coenzyme domain	0.65 (0.42)[a]	0.78 (0.33)
catalytic domain	1.13 (0.52)	0.44 (0.33)
both domains	1.76 (1.53)	1.25 (1.15)
AB dimer	1.99 (1.70)	2.03 (1.95)
AC dimer	2.04 (1.77)	−
AD dimer	1.80 (1.57)	−

[a] The values in parentheses refer to superimpositions which exclude the most deviating C^{α} atoms (see the text for details on the selections).

be observed in the C^{α} atom rmsds of pairwise superimposed subunits of SsADH apo and holo tetramer structures. The rmsd on all selected C^{α} atoms of the AC dimers is indeed higher than the value calculated for AD dimers, which is in turn comparable to that obtained when the C^{α} atoms of the A subunits of apo and holo structures are superimposed.

A crucial role is played at the tetramer interfaces by helix α4 whose position is practically unaltered when going from the apo to the holo form in SsADH. This is one of the main differences with the HLADH structure. In fact, the analysis of the rigid-body rotation observed in the apo−holo transition of the SsADH and HLADH A subunits shows that the axes are located in different positions. Compared to that in HLADH, the rotation axis in SsADH is shifted toward the periphery of the subunit, passing very close to the α4 helix (Figure 1). The axis is closer to the backside of subunit A, which is the side that in tetrameric SsADH interacts with subunits C and D, whereas in dimeric HLADH, it interacts with the solvent. In SsADH, the axis shift results in smaller local displacements of some of the regions at the subunit interface when going from the apo to the holo conformation.

The different position of the rotation axis in SsADH and HLADH also has a different effect on AB dimer assembly. Indeed, the AB dimer in HLADH appears to be more flexible than in SsADH. This can be ascertained from the rmsd on C^{α} atoms of the superimposed AB dimers in apo- and holo-SsADH. The rmsd value is 1.70 Å which is only slightly higher than the rmsd of 1.53 Å obtained when superimposing only the A subunits. On the other hand, in HLADH structures, the corresponding rmsd value for the AB dimer superposition is 1.95 Å, substantially higher than the value of 1.15 Å obtained for the A monomer alignment. This

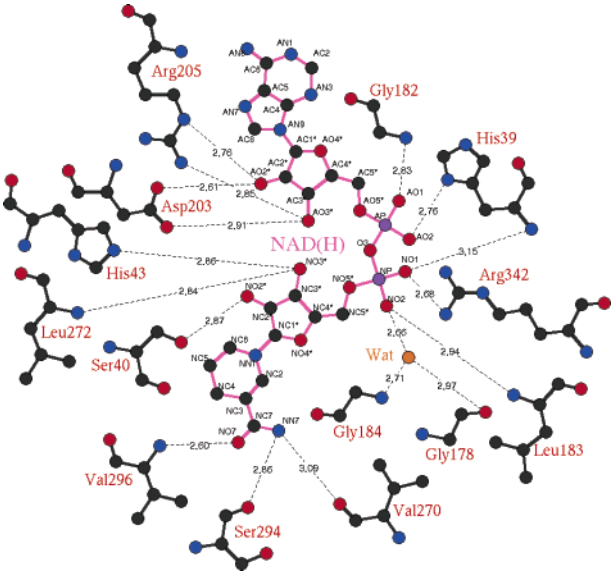

FIGURE 2: Schematic diagram of H-bond interactions of the NAD(H) molecule in subunit A. This figure was generated using Ligplot (*46*). The structurally conserved water molecule in the Rossmann fold (*22*) has been highlighted in peach.

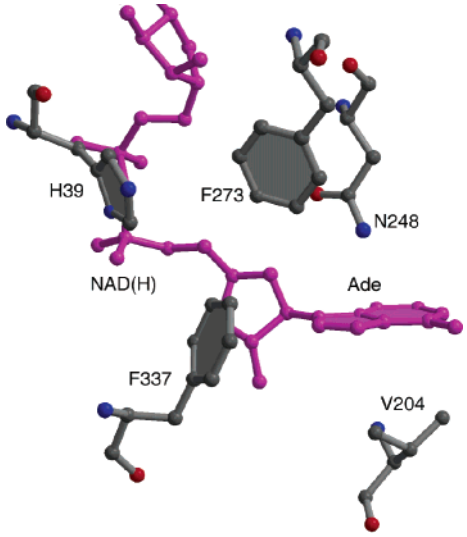

FIGURE 3: Interactions with the NAD(H) coenzyme. The amino−aromatic interaction between Asn248 and the adenine base is shown. The aromatic side chains protecting the coenzyme from the solvent (toward the observer) are also shown. This figure was prepared by using BobScript (*47*) and Raster3D (*45*).

indicates that in HLADH the reorganization of the dimer assembly, upon coenzyme binding, reflects only in part the conformational change due to the rigid-body rotation of the catalytic domains toward the coenzyme-binding domains.

Coenzyme Binding Interactions. The coenzyme is very well ordered in both subunits. It adopts an extended conformation similar to NADH bound to mammalian ADH with both riboses in the 2′-endo puckering conformation. As expected, Asp203 is hydrogen-bonded to the O atoms of the adenine ribose moiety (Figure 2). The aspartate residue is indeed one of the primary determinants of the NAD(H) specificity. The other determinant is the glycine-rich sequence motif which in SsADH corresponds to the ^{178}-GAGGGLG^{184} segment.

This segment displays direct H-bonds with the pyrophosphate moiety or H-bonds via a very structurally conserved water molecule (*22*) (Figure 2). The pyrophosphate group also interacts with two basic residues, Arg342 and His39, which correspond to two arginines in HLADH (Arg367 and Arg47, respectively). His39 changes conformation from the apo to the holo form to avoid clashing with the pyrophosphate.

On the basis of the apo structure, it was suggested that the negative charge of the coenzyme could also be counterbalanced by the positive charge of the Arg205 side chain which was completely disordered in the absence of the NAD(H) molecule. In the holo form indeed, a well-defined density for Arg205 is observed. The side chain displays bifurcated H-bonds with the ribose oxygens of the adenosine moiety and is 5−6 Å from the pyrophosphate group.

The adenine moiety is the only part of the coenzyme exposed to solvent. In most ADH structures, the ring is sandwiched between two hydrophobic side chains making van der Waals interactions below and above the ring plane (*23*). However, in SsADH, one of these two positions is occupied by Val204 while the other is occupied by Asn248. The latter residue orients its side chain N atom toward the ring (3.05 Å) to make an amino−aromatic interaction involving the partial positive charge $\delta+$ of the Asn NH_2 group and the $\delta-$ π electrons of the aromatic ring (Figure 3).

The carboxamide group anchors the nicotinamide ring to the main chain nitrogen of residue Val296 and the main chain carbonyl oxygens of residues Ser294 and Val270, analogous to NADH binding to other ADHs in the closed conformation. The ribose on the nicotinamide side is hydrogen bonded to the side chains of Ser40 and His43 as well as to the main chain of Leu272.

The nicotinamide ring is also tightly bound by hydrophobic interactions with the side chains of Val270, Thr153, and Leu183, which make contact with the unreactive face of the ring with distances of less than 4.0 Å. The other face is directed toward the active site and is close to the catalytic zinc ion and its ligands.

Further hydrophobic interactions contribute toward locking the NADH molecule into the interdomain cleft. In fact, the side chains of Phe273 and Phe337, on the opposite side of the cleft, close around the NADH by interacting with each other within 4.0 Å. The aromatic rings also make van der Waals interactions with the adenine base edge, isolating the pyrophosphate group and the riboses from the solvent (Figure 3).

Catalytic and Substrate Binding Site. The catalytic zinc exhibits a tetracoordinate environment with three ligands contributed by the enzyme (Cys38, Cys154, and His68) and a 2-ethoxyethanol molecule occupying the fourth coordination position (Figure 4). In the apoenzyme, the fourth zinc ligand was the highly conserved Glu69, located in a cavity opposite the substrate site (*7*). In the holo structure presented here, the Glu69 side chain is 5.1 Å from the zinc. The Glu69 carboxylate oxygen atoms make bifurcated H-bond interactions with N atoms of the Arg342 guanidinium group. In addition, Glu69 $O^{\epsilon 2}$ is H-bonded to the main chain N of Ser155 (Figure 4). The Glu69 $O^{\epsilon 2}$ atom in the apo structure is directly bonded to the zinc, whereas $O^{\epsilon 1}$ displays an H-bond with the Arg342 side chain.

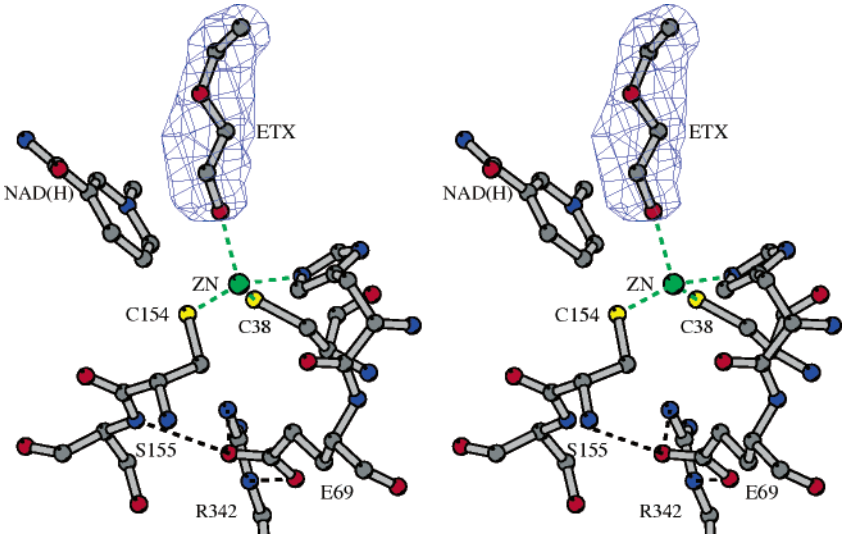

FIGURE 4: Tetrahedral coordination of the catalytic zinc in the A subunit. The covalent bonds of the four ligands are shown as dashed green lines. Part of the NAD(H) molecule is also shown as well as some interactions involving neighboring residues (see the text). The $F_o - F_c$ omit map density for the 2-ethoxyethanol molecule (ETX) is contoured at 4.0σ.

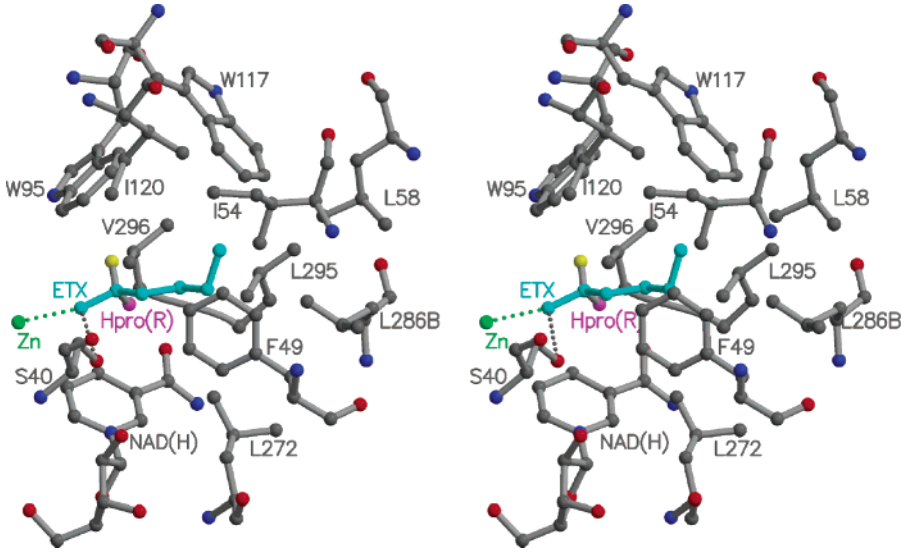

FIGURE 5: Substrate hydrophobic channel. The 2-ethoxyethanol molecule (ETX) is depicted in cyan, whereas the two hydrogen atoms on the C1 atom are shown in magenta (pro-*R*) and yellow (pro-*S*). The interactions with the active site zinc and Oγ of Ser40 are represented by dotted lines.

The ethoxyethanol molecule is coordinated to the zinc ion via its hydroxyl oxygen atom. The Zn−O distance is 2.3 and 2.4 Å in the A and B subunit, respectively, resulting in a more continuous electron density around the zinc in the A subunit. Despite the rather large shape of the electron density, a single orientation of the substrate was confidently defined. The ethoxyethanol molecule is positioned quite appropriately for hydride transfer. The hydride-donating methylene carbon, C1, on the 2-ethoxyethanol is 3.7 Å from the accepting carbon, C4, on the nicotinamide ring. The pro-*R* hydrogen of C1 is pointing almost directly toward the C4 position of the coenzyme (Figure 5). The ethoxyethanol oxygen also forms an H-bond to Ser40, which in turn hydrogen bonds to the O2′ ribose hydroxyl oxygen of the cofactor. By analogy with HLADH, SsADH Ser40 and His43 should form the putative relay system for transport of the alcohol hydroxyl proton to solvent. The hydrogen bond between His43 and the ribose O3′ completes this relay system in SsADH (Figure 2). The substrate is also held in its site by several hydrophobic interactions which are listed in Table 4.

Table 4: Substrate Contacts

2-ethoxyethanol interacting atom	residue interacting with protein[a]
O1	**Ser40**
C1	Val296, Trp95
C2	Leu272, Ile120, Phe49
O2	*Leu272, Leu295*
C3	Phe49, Leu272, Leu286B[b]
C4	Phe49, Trp117, Ile120, Leu286B[b]

[a] The H-bond contact is shown in bold, whereas in lightface type are listed the hydrophobic contacts between C atoms that are less than 4.5 Å long. Destabilizing contacts between O and C atoms are shown in italics. [b] Except for this residue, all the other residues belong to the A subunit.

DISCUSSION

Domain Closure and Loop Displacement. All the structurally studied medium chain ADHs from eukaryotic sources undergo a substantial conformational change in the tertiary structure upon coenzyme binding. The coenzyme, the first

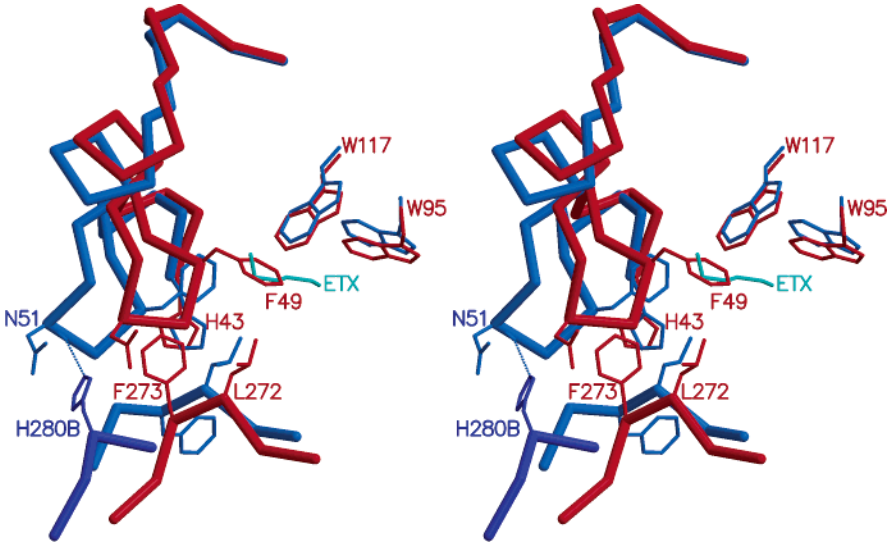

FIGURE 6: Loop movement upon coenzyme and substrate binding. Residues 43−65 and 270−275 are shown for the apo (red) and holo (blue) SsADH forms. The ethoxyethanol molecule is shown in cyan. To highlight the structural change of residues 46−62 within the catalytic domain, the two structures are superimposed by using the catalytic domains. Thus, the nonalignment of residues 270−275 reflects the rigid-body rotation of the domains. In the holo structure, residues 278−281 of subunit B (dark blue) are also indicated in the figure to show the H-bond between the N atom of the main chain of residue Asn51A and the NE2 atom of residue His280B.

ligand to bind, induces a movement of the catalytic domain toward the coenzyme-binding domain which can be best described as a rigid-body rotation (*24*). This conformational change narrows the interdomain cleft, brings the cofactor closer to the substrate, and isolates the active site from the solvent, as required for the hydride transfer.

The extent of domain closure in eukaryotic ADH structures determined so far can vary from the 5−7° rotation [class II mouse liver ADHs (*5*), class I cod liver ADHs (*25*), and human ADHs (*3*)] to the 10° rotation, the largest domain motion, observed in HLADH. On the other hand, the structures of bacterial ADHs from *Clostridium beijerinckii* and *Thermoanaerobacter brockii* (*6*) reveal only a 2.5° domain closure when comparing the apo and holo binary complex forms. Spectroscopic studies on TbADH were in line with the crystallographic results by showing the lack of any significant conformational change in the tertiary structure of TbADH upon coenzyme binding (*26*). On the basis of this observation and further evidence that will be mentioned later, the possibility of a different mechanism of action between bacterial and mammalian ADHs was proposed. In this context, the finding of an 11° domain closure displayed by the SsADH−NADH−ETX complex relative to the apo-SsADH structure makes the archaeal enzyme more similar to eukaryotic than to bacterial ADHs.

The values of the rigid-body rotation angle for SsADH and HLADH are similar; nevertheless, the rotation axis is differently positioned. In SsADH, the shift of the axis toward the periphery of the subunit, at the tetramer interface, yields a larger movement of the more distant regions from the axis such as the ones at the front side of the subunit. As a result, despite the more open cleft found in the SsADH apoenzyme relative to that in the HLADH apoenzyme (*7*), an efficient closure of the SsADH holoenzyme interdomain cleft can be achieved by the same degree of rigid-body rotation as in HLADH.

The domain closure in SsADH is also accompanied by a structural rearrangement of some loop regions in the catalytic and coenzyme-binding domains, as observed also for the HLADH enzyme (*21*). In particular, in the coenzyme-binding domain, residues 271−275 undergo a local conformational change in the holo form as compared to the apo form. This segment rearranges by pointing toward the bottom of the NAD cleft, making room for the loop of residues 46−62 on the opposite domain to come closer to the coenzyme-binding domain. The region of residues 270−275 interacts with an NADH molecule, with Asn248 and Asn249 in the coenzyme-binding domain, and with Phe49 and Gly50 in the catalytic domain.

At one end of the region of residues 271−275, Val270 is H-bonded to the coenzyme molecule while adopting quite similar positions in the apo and holo forms. On the other hand, Leu272, which undergoes a large rearrangement, has a hydrogen bond from its backbone NH group to an oxygen atom of the pyrophosphate. The side chains of Val270 and Leu272 form van der Waals contacts with the NAD ring, and Gly271 and Phe273 form van der Waals contacts with the nicotinamide ribose. Because of its high flexibility, Gly274 rearranges its conformation, acting as a switch for a substantial structural reorganization of residue Phe273 in the holo form. This Phe side chain protrudes toward the bottom of the cleft to interact with Phe337 and His39 on the other domain, thus serving as a clip to lock the NADH into the cleft isolating it from the solvent (Figure 3). As already suggested for Phe273 on the basis of the apoenzyme structure (*27*), the present holo structure highlights the role played by these aromatic residues in NADH binding, thus explaining the unusual position of these Phe residues on solvent-exposed loops.

Furthermore, the movement of Phe273, from the apo to the holo form, allows loop 46−62 to rearrange and extensively interact, through a complementary hydrophobic surface, with the helix region of residues 280−286 of the near subunit B. This interface is lined by residues Pro282B, Leu283B, Thr285B, and Leu286B. Indeed the loop 46−62 conformation, in the holo form, generates the room to accommodate the imidazole ring of His280B which becomes less exposed (Figure 6).

In HLADH, the substitutions within loop 292−298 (corresponding to residues 271−275) or at the end of the loop were suggested to perturb the equilibrium of the conformational change of the enzyme−coenzyme complex (*11*, *28*). Also in the SsADH mutant, N249Y, structural alterations in loop 271−275 induced by the substitution in adjacent loop 248−250 were correlated to the observed decrease in affinity for coenzymes (*27*).

The movement of loop 271−275 is correlated with the movement of loop 46−62, which not only moves together with the entire catalytic domain toward the other domain but also displays a drastic change within its internal domain during the apo−holo transition (Figure 1A). The two loops lock themselves together by van der Waals contacts between C^{α} atoms of Gly50 and Gly274 (3.6 Å) and between side chains of Phe49 and Leu272 (3.6 Å). A water-mediated contact between Leu272 and Gly50 is also formed. In addition, loop 46−62 is anchored by the interaction between the main chain of Asn51 and the side chain of His280 in subunit B (Figure 6). Segment 46−62 is one of the most flexible parts of the SsADH structure. It was found to be very disordered in the mutant N249Y apo structure where the conformational changes induced by the mutation probably altered the hydrophobic interactions of side chains at this domain interface. The loop becomes stabilized in the holo form, and is displaced to open the entrance gate of the substrate channel which was severely restricted in the apo form (*7*) (see the discussion below).

The correlated motion of the two loops, 271−275 and 46−62, in the SsADH apo−holo transition is confirmed by the structure presented here. With respect to this feature, the HLADH enzyme behaves somewhat differently. Indeed, corresponding loops 292−298 and 51−58 display a smaller contact area than in SsADH, and although a significant conformational change occurs at loop 292−298, residues 51−58 do not undergo a displacement within the catalytic domain as large as that observed in SsADH.

Coenzyme Binding. The coenzyme binds to SsADH in a manner similar to that in which it binds HLADH, with an extended conformation and both riboses in the 2′-endo puckering conformation (*23*). As in HLADH, in SsADH the carboxamide group of the nicotinamide interacts by three H-bonds with protein main chain atoms (Figure 2). These cofactor hydrogen bonds are found in all closed form complexes of HLADH with either the coenzyme or coenzyme analogues. Since complexes of HLADH with NAD analogues, which lack the carboxamide group or the nicotinamide ring, crystallize in the open form, it was proposed that these H-bonds are required for maintenance of the closed conformation of the enzyme (*23*, *29*−*31*). In line with this suggestion, the SsADH holo structure preserves these H-bonds, whereas bacterial ADHs do not. The above interactions can be important because of their role in stabilizing the *anti* conformation of the NAD ring relative to the ribose sugar; this *anti* conformation is also crucial for the stereospecificity of hydride transfer. The *syn* conformation of the NAD ring, corresponding to an ∼180° rotation around the *N*-glycosidic bond, sterically interferes with the active site center (Zn ion and its ligands) in the closed form. Under the assumption of an equilibrium between open and closed forms of ADH even in the presence of the coenzyme, the stabilization of the *anti* conformation against the *syn* conformation of the NAD ring favors the closed form of the enzyme.

The mobility of the NAD base is also restricted by hydrophobic interactions mainly with the side of the ring not involved in hydride transfer. Side chains of Thr153, Leu183, and Val270 make close contacts (within 4.0 Å) with the ring, acting as a sticky patch for it. Corresponding residues are observed in HLADH at the backside of the NAD ring, namely, Thr178, Val203, and Val292. Amino acid substitutions at these sites in HLADH have been shown to significantly alter the kinetics of the enzyme and increase the dissociation constants for coenzymes as compared to those of the wild-type protein (*28*, *32*). Replacing Val and Thr with less bulky residues also produced a significant, although modest, decrease in the rate constant for hydride transfer from benzyl alcohol (*32*). This effect was explained by both the decrease in the number of steric interactions with the NAD ring and the perturbation of the dynamics of the protein and the nicotinamide ring, which resulted in a nonoptimal relative orientation of the hydride donor and acceptor for the hydride transfer. An analogous role for the corresponding SsADH residues can be suggested on the basis of the close similarity of the interactions with the NAD ring between the two enzymes.

Only a few NADH−protein interactions in SsADH differ from those in HLADH, and they include the amino−aromatic interaction involving the adenine ring and Asn248 as well as the additional H-bond between Gly182 N and one of the oxygen atoms of the pyrophosphate (Figure 2). The former interaction, involving the partial positive charge carried by the Asn amino group and the adenine π electron cloud, is quite unusual in the ADH enzyme family. On the other hand, a statistical survey has recently shown the frequent occurrence of amino acid−nucleobase cation−π interactions in protein structures (*33*). In SsADH, the angle between the aromatic plane of the adenine and that formed by the amide group of Asn248 is ∼78°, indicating a T-shaped conformation which is usually less frequent than the stacked conformation (*33*).

Catalytic Zinc Coordination. The structure of the SsADH ternary complex shows a tetrahedral coordination of the zinc ion which is ligated to three protein ligands (Cys154, Cys38, and His67) and to the hydroxyl group of the 2-ethoxyethanol. There is indeed a change in the coordination environment relative to the apoenzyme where there is an endogenous ligand, Glu69, directly bound to the zinc (Figure 4).

In the apo−holo transition, the configuration of the zinc is inverted since the ion is displaced toward the substrate site and away from the Glu69 side chain. When the catalytic domains of the apo and holo form are aligned, the active site zinc is found to be displaced 1.75 Å from its position in the apoenzyme. This movement could be the consequence of the changes induced by the binding of the coenzyme and/or of the substrate.

Among the four zinc ligands, Cys38 exhibits the largest change in conformation of both the main and side chain. This change can be favored by the rearrangement of the adjacent residue, His39, which is shifted and reoriented to avoid clashing with the NAD(H) molecule and to directly bind to the pyrophosphate group. Concurrently, Arg342 changes its orientation, extending its side chain to interact with the pyrophosphate of NAD(H). As a result, the H-bond

between Arg342 NH2 and Ser155 OG is broken, whereas an additional interaction is formed between Arg342 and the side chain of Glu69 which undergoes a slight rotation. In fact, one of the carboxylate oxygens of Glu69 swings away from the zinc direction, pointing toward the main chain N of Ser155 with which it forms a hydrogen bond. This backbone nitrogen in the apo structure was H-bonded to the O of Pro151 connecting the Ser residue in the α-helix conformation to the Pro residue in a 3_{10}-turn.

Drawn by these subtle changes in the holo form as well as by the presence of the alcohol in the substrate site, the zinc ion is positioned slightly out of the plane formed by the coordinating atoms of its three protein ligands, and it can ligate to the hydroxyl group of 2-ethoxyethanol.

The role, if any, in ADH catalysis played by the Glu residue next to the His zinc ligand is still unclear. This acidic residue is very well conserved among ADHs. An important role for this residue was first envisaged by studies on yeast ADH which showed that substitution of Glu with Gln resulted in a severe loss in enzyme activity (*34*). In addition, theoretical calculations on the HLADH enzyme indicated that the Glu residue can intermittently coordinate to the zinc during catalysis to facilitate the ligand exchange at the catalytic center (*35*). A similar mechanism was also proposed for a class III member of the ADH family, namely, the formaldehyde dehydrogenase, on the basis of several crystal structures determined for this enzyme (*4*, *36*).

The X-ray structures of some other ADH family members, in their apo forms or in binary or ternary complexes, showed the Glu directly bound to the zinc (*9, 37*). In particular, in bacterial ADHs, the binding of Glu60 to the catalytic zinc in the apo and holo forms was observed (*6*). This new ligation state of the zinc was taken to be a further difference with HLADH, supporting the proposal of a different mechanism of action for bacterial ADHs relative to mammalian ones. However, a very recent mutagenesis study carried out on TbADH in which Glu60 was replaced with Ala and Asp indicated that the catalytic efficiency of these mutants is only slightly affected (*38*). Although the Glu residue is found to be nonessential for TbADH catalysis, X-ray absorption studies support a dynamic role for this residue which is found to be involved in pentacoordinated intermediate states during TbADH turnover (*12*). It has been suggested that in the absence of the Glu, the role of coordinating the zinc to facilitate the exchange of ligands can be played by a water molecule.

The change in the ligation state of Glu69 in the two SsADH structures, corresponding to two snapshots of different steps along the catalytic cycle, provides additional evidence of the dynamic role of the conserved glutamate residue in ADHs. A more complete picture for SsADH must await the structural determination of the binary complex as well as site-directed mutagenesis studies.

Substrate Binding Site and Stereospecificity. SsADH is active toward a variety of alcohol substrates, both aromatic and aliphatic ones, the latter being either primary or secondary alcohols (*39*). The substrate binding site consists of an elongated channel with hydrophobic residues projecting from all sides and with the catalytic zinc ion at the bottom of the channel (Figure 5).

In ADHs, the substrate pocket can be accessed from two directions: the front side of the subunit via the interdomain cleft, which is closed once the NAD(H) is bound, and the top side of the subunit. In the SsADH apo form, the access through the latter gate was found to be restricted by the conformation of loop 46−62 which extends to cover the active site. In particular, in the apo form, the Phe49 side chain directly interacts with Trp95 and Trp117, thus forming an aromatic cluster (*7*) and occupying the same position as the substrate molecule in the ternary complex structure presented here (Figure 6). Residues 46−62 in the holo form essentially move as a rigid body within the catalytic domain, moving away from the active site and toward loop 270−275 on the coenzyme-binding domain (Figure 6). Indeed, in a manner different from that in HLADH, the apo−holo domain closure in SsADH is coupled with a substantial movement of the region near the mouth of the active site, suggesting that the flexibility of these regions is an important factor in enzyme catalysis.

The volume of the substrate site is quite large, allowing for the binding of bulk substrates such as substituted or unsubstituted cyclohexanol and benzyl alcohol. In the structure presented here, the pro-*S* hydrogen of the substrate projects toward the Trp region, whereas the pro-*R* hydrogen is oriented toward the NAD(H) ring. On the same side of NAD(H), there is the Ser40 side chain directly H-bonded to the hydroxyl group of the substrate.

Most of the 2-ethoxyethanol atoms make van der Waals contacts (interatomic C−C distance of less than 4.0 Å) with some of the channel-forming hydrophobic residues, as shown in Table 4. For primary alcohol substrates, the decrease in K_m values as the carbon chain length increases (Table 2) is consistent with these favorable interactions between the hydrophobic region of the enzyme and the carbon skeleton of the substrate.

The stereospecificity of the enzyme for the oxidation of secondary alcohols can be explained on the basis of this ternary complex structure. SsADH preferentially oxidizes (*S*)-2-butanol rather than (*R*)-2-butanol, the catalytic efficiencies being 300 and 5 mM^{-1} s^{-1}, respectively (*39*). The (*S*)-2-butanol has been modeled into the binding site with the hydrogen of the C2 atom pointing toward the NAD ring. As a result, the larger alkyl substituent (ethyl group) extends into the large channel, superimposing on the carbon chain of 2-ethoxyethanol. On the other hand, the smaller alkyl substituent (methyl group) replaces the substrate pro-*S* hydrogen occupying a smaller hydrophobic pocket formed by the side chains of Trp95 and Val296 (Figure 5). The (*S*)-2-butanol methyl group shows a steric clash with the Trp95 ring, but a slight reorientation of the aromatic side chain is sufficient to turn it into a favorable hydrophobic interaction. On the other hand, when the *R*-enantiomer is modeled, a poorer steric fit results, since the larger group is now in the smaller pocket, and vice versa.

Trp95 plays the same role as Phe93 in HLADH which is mainly responsible for binding the substrates in an orientation which facilitates hydride transfer of the pro-*R* hydrogen (*40*). Kinetic and crystallographic studies on the F93A substituted HLADH enzyme suggested that removing the steric interactions of the aromatic side chain increases the mobility of substrate and hence decreases the likelihood that the alcohol

will be oriented in the correct conformation for hydride transfer (*41*).

The higher steric hindrance in the region including Trp95 and Val296 side chains also prevents the binding in this site of a branched chain such as that of an isopropyl group. This can explain the stereoselectivity of the product obtained by the oxidation of 3-methylbutan-2-one. In fact, the *S*-enantiomer of the corresponding alcohol is produced by an ~100% optical yield (*39*), indicating that the ketone isopropyl substituent can only point into the channel, whereas the ketone methyl substituent points toward the Trp side.

Proton Relay System. On the basis of kinetic and structural studies on horse and human class I ADHs, it was suggested that the proton of the alcohol, which dissociates in a hydrophobic environment, is transferred to the bulk solvent by a series of H-bonds forming a proton relay system (*21*). The hydrogen bond network involves the Ser/Thr residue that hydrogen bonds to the alcohol oxygen atom, the hydroxyl groups of nicotinamide ribose, and a general base exposed to solvent which is usually a His residue.

Although bacterial ADHs contain the corresponding Ser and His residues, these side chains were not properly oriented to form the proton shuttle in the binary complex structures (*6*). On the other hand, in the SsADH ternary complex, the proton shuttle is fully formed and involves both ribose hydroxyl groups. The hydrogen-bonded relay series is as follows: ROH···Ser40 O^{γ}···ribose 2′-OH···ribose 3′-OH···His43 $N^{\epsilon 2}$···H_2O.

The essential role of the His residue has been debated because of the absence of this residue in some members of the ADH family (*5*, *25*), and because of the only 10-fold decrease in activity of the HLADH enzyme upon substitution of His with Gln (*42*). A recent molecular dynamics study on HLADH succeeded in identifying an alternative route for proton transfer to solvent, in the absence of His51 (*43*). A pathway was found which involves ribose 3′-OH and Ile269. The 3′-OH is hydrogen bonded to the Ile269 carbonyl O which maintains this proton in a position to be transferred to water. Compared to HLADH, the SsADH structure shows no H-bond acceptor near the 3′-OH of ribose. On the basis of these MD studies, it can be surmised that this alternative pathway is less favored and that His43 is a more critical residue for the enzyme activity, compared to His51 of HLADH. However, this deserves site-directed mutagenesis experiments.

ACKNOWLEDGMENT

We acknowledge the European Synchrotron Radiation Facility for providing the synchrotron radiation facilities, and we thank the beamline ID14-4 staff for their assistance during data collection. Giosuè Sorrentino, Maurizio Amendola, and Gabriella Boscaino are acknowledged for their assistance.

NOTE ADDED IN PROOF

While this paper was under revision, the crystal structure of a ternary complex of an archaeal ADH, whose crystallization has been cited in this paper (*8*), has been reported [PDB entry 1H2B (*48*)].

REFERENCES

1. Nordling, E., Persson, B., and Jornvall, H. (2002) *Cell. Mol. Life Sci. 59*, 1070−1075.
2. Branden, C. I., Jornvall, H., Eklund, H., and Furugren, B. (1975) *Alcohol dehydrogenases*, Vol. 11, Academic Press, New York.
3. Niederhut, M. S., Gibbons, B. J., Perez-Miller, S., and Hurley, T. D. (2001) *Protein Sci. 10*, 697−706.
4. Sanghani, P. C., Robinson, H., Bosron, W. F., and Hurley, T. D. (2002) *Biochemistry 41*, 10778−10786.
5. Svensson, S., Hoog, J. O., Schneider, G., and Sandalova, T. (2000) *J. Mol. Biol. 302*, 441−453.
6. Korkhin, Y., Kalb, A. J., Peretz, M., Bogin, O., Burstein, Y., and Frolow, F. (1998) *J. Mol. Biol. 278*, 967−981.
7. Esposito, L., Sica, F., Raia, C. A., Giordano, A., Rossi, M., Mazzarella, L., and Zagari, A. (2002) *J. Mol. Biol. 318*, 463−477.
8. Guy, J. E., Isupov, M. N., and Littlechild, J. A. (2003) *Acta Crystallogr. D59*, 174−176.
9. Karlsson, A., El-Ahmad, M., Johansson, K., Shafqat, J., Jornvall, H., Eklund, H., and Ramaswamy, S. (2003) *Chem. Biol. Int. 143−144*, 239−245.
10. Cedergren-Zeppezauer, E. S., Andersson, I., Ottonello, S., and Bignetti, E. (1985) *Biochemistry 24*, 4000−4010.
11. Ramaswamy, S., Park, D. H., and Plapp, B. V. (1999) *Biochemistry 38*, 13951−13959.
12. Kleifeld, O., Frenkel, A., Martin, J. M., and Sagi, I. (2003) *Nat. Struct. Biol. 10*, 98−103.
13. Meijers, R., Morris, R. J., Adolph, H. W., Merli, A., Lamzin, V. S., and Cedergren-Zeppezauer, E. S. (2001) *J. Biol. Chem. 276*, 9316−9321.
14. Cannio, R., Fiorentino, G., Carpinelli, P., Rossi, M., and Bartolucci, S. (1996) *J. Bacteriol. 178*, 301−305.
15. Pearl, L., Demasi, D., Hemmings, A. M., Sica, F., Mazzarella, L., Raia, C. A., D'Auria, S., and Rossi, M. (1993) *J. Mol. Biol. 229*, 782−784.
16. Otwinowski, Z., and Minor, W. (1997) *Methods Enzymol. 276*, 307−326.
17. Navaza, J. (1994) *Acta Crystallogr. A50*, 157−163.
18. Brunger, A. T., Adams, P. D., Clore, G. M., DeLano, W. L., Gros, P., Grosse-Kunstleve, R. W., Jiang, J.-S., Kuszewski, J., Nilges, M., Pannu, N. S., Read, R. J., Rice, L. M., Simonson, T., and Warren, G. L. (1998) *Acta Crystallogr. D54*, 905−921.
19. Jones, T. A., Zou, J. Y., Cowan, S. W., and Kjeldgaard, M. (1991) *Acta Crystallogr. A47*, 110−119.
20. Laskowski, R. A., MacArthur, M. W., Moss, M. D., and Thorton, J. M. (1993) *J. Appl. Crystallogr. 26*, 283−291.
21. Eklund, H., and Branden, C.-I. (1987) in *Biological Macromolecules and Assemblies*, pp 73−142, Wiley-Interscience, New York.
22. Bottoms, C. A., Smith, P. E., and Tanner, J. J. (2002) *Protein Sci. 11*, 2125−2137.
23. Eklund, H., Samama, J. P., and Jones, T. A. (1984) *Biochemistry 23*, 5982−5996.
24. Colonna-Cesari, F., Perahia, D., Karplus, M., Eklund, H., Braden, C. I., and Tapia, O. (1986) *J. Biol. Chem. 261*, 15273−15280.
25. Ramaswamy, S., el Ahmad, M., Danielsson, O., Jornvall, H., and Eklund, H. (1996) *Protein Sci. 5*, 663−671.
26. Kleifeld, O., Frenkel, A., Bogin, O., Eisenstein, M., Brumfeld, V., Burstein, Y., and Sagi, I. (2000) *Biochemistry 39*, 7702−7711.
27. Esposito, L., Bruno, I., Sica, F., Raia, C. A., Giordano, A., Rossi, M., Mazzarella, L., and Zagari, A. (2003) *FEBS Lett. 539*, 14−18.
28. Rubach, J. K., Ramaswamy, S., and Plapp, B. V. (2001) *Biochemistry 40*, 12686−12694.
29. Samama, J. P., Zeppezauer, E., Biellmann, J. F., and Branden, C. I. (1977) *Eur. J. Biochem. 81*, 403−409.
30. Samama, J. P., Wrixon, A. D., and Biellmann, J. F. (1981) *Eur. J. Biochem. 118*, 479−486.
31. Li, H., Hallows, W. H., Punzi, J. S., Pankiewicz, K. W., Watanabe, K. A., and Goldstein, B. M. (1994) *Biochemistry 33*, 11734−11744.
32. Rubach, J. K., and Plapp, B. V. (2003) *Biochemistry 42*, 2907−2915.
33. Biot, C., Buisine, E., Kwasigroch, J.-M., Wintjens, R., and Rooman, M. (2002) *J. Biol. Chem. 277*, 40816−40822.
34. Ganzhorn, A. J., and Plapp, B. V. (1988) *J. Biol. Chem. 263*, 5446−5454.
35. Ryde, U. (1995) *Proteins 21*, 40−56.
36. Sanghani, P. C., Bosron, W. F., and Hurley, T. D. (2002) *Biochemistry 41*, 15189−15194.

37. Johansson, K., El-Ahmad, M., Kaiser, C., Jornvall, H., Eklund, H., Hoog, J. O., and Ramaswamy, S. (2001) *Chem. Biol. Int. 130*−*132*, 351−358.
38. Kleifeld, O., Shi, S. P., Zarivach, R., Eisenstein, M., and Sagi, I. (2003) *Protein Sci. 12*, 468−479.
39. Raia, C. A., Giordano, A., and Rossi, M. (2001) *Methods Enzymol. 331*, 176−195.
40. Eklund, H., Plapp, B. V., Samama, J. P., and Branden, C. I. (1982) *J. Biol. Chem. 257*, 14349−14358.
41. Rubach, J. K., and Plapp, B. V. (2002) *Biochemistry 41*, 15770−15779.
42. Ehrig, T., Hurley, T. D., Edenberg, H. J., and Bosron, W. F. (1991) *Biochemistry 30*, 1062−1068.
43. Luo, J., and Bruice, T. C. (2001) *J. Am. Chem. Soc. 123*, 11952−11959.
44. Kraulis, P. J. (1991) *J. Appl. Crystallogr. 24*, 946−950.
45. Merritt, E. A., and Bacon, D. J. (1997) *Methods Enzymol. 277*, 505−524.
46. Wallace, A. C., Laskowski, R. A., and Thornton, J. M. (1995) *Protein Eng. 8*, 127−134.
47. Esnouf, R. M. (1999) *Acta Crystallogr. D55*, 938−940.
48. Guy, J. E., Isupov, M. N., and Littlechild, J. A. (2003) *J. Mol. Biol. 331*, 1041−1051.

BI035271B